

Impact of urban expansion on land surface temperature and carbon emissions using machine learning algorithms in Wuhan, China

Maomao Zhang^{a,*}, Abdulla - Al Kafy^b, Pengnan Xiao^c, Siyu Han^a, Shangjun Zou^a, Milan Saha^{d,e}, Cheng Zhang^f, Shukui Tan^{a,*}

^a College of Public Administration, Huazhong University of Science and Technology, Wuhan 430079, China

^b Department of Geography & the Environment, The University of Texas at Austin, Austin, TX 78712, USA

^c College of Urban and Environmental Sciences, Central China Normal University, Wuhan 430079, China

^d Department of Urban & Regional Planning, Bangladesh University of Engineering & Technology (BUET), Dhaka 1312, Bangladesh

^e School of Environmental Science and Management, Independent University Bangladesh, Dhaka 1312, Bangladesh

^f School of Mechanical Science and Engineering, Huazhong University of Science and Technology, Wuhan 430074, China

ARTICLE INFO

Keywords:

Urban expansion
Thermal environment
Carbon emission
ANN-CA
IWOA-LSTM
China

ABSTRACT

The impact of the rapid expansion of urban land on the urban thermal environment and carbon chain has attracted widespread attention. This paper uses artificial neural network-cellular automata (ANN-CA) and long short-term memory model of the improved whale optimization algorithm (IWOA-LSTM) models to predict the changes of LULC and LST, and explores the correlation between LST and carbon emissions in Wuhan. The results show that urban land will occupy >70.05% of the central urban area, while green land and water areas will continue to decrease to varying degrees in 2030 and 2040. The area of the high temperature area ($LST > 30^{\circ}\text{C}$) is expanding in the urban land, while the green land and the low temperature area of the water body are gradually shrinking. The area of high temperature is expanding, and the area with $LST > 30^{\circ}\text{C}$ accounts for 67.84% in summer, and the area with LST at $10^{\circ}\text{C} \sim 15^{\circ}\text{C}$ accounts for 96.32% in winter. The fitting results of correlation regression show that there is a significant correlation between carbon emissions and LST. The R^2 of linear fitting between LST and carbon emissions in summer and winter of 2000 are 0.6227 and 0.6143, respectively. The R^2 of linear fitting in summer and winter is higher, both of which are >0.85 in 2010 and 2020. This research may provide new clues for future urban development and thermal environment governance and carbon emission mitigation.

1. Introduction

The development of urbanization has added a lot of vitality to cities, but the excessive expansion of urban land has also aggravated the deterioration of urban thermal environment (Rao et al., 2021; Gao and Yuan, 2022; Li et al., 2022). The process of urbanization has also prompted many cities that focus on plane development to transform into an urbanization mode that coexists with plane expansion and three-dimensional development (Zhao et al., 2020; Rao et al., 2020). Excessive urbanization may lead to a higher building area

* Corresponding authors.

E-mail addresses: Star_mzhang@mails.ccnu.edu.cn, zhangmaomao516@126.com (M. Zhang), tansk@hust.edu.cn (S. Tan).

ratio in the city, which makes the heat collected in the city difficult to diffuse, and accelerates the intensity of the urban heat island(Fu et al., 2022; Shaker et al., 2019; Stewart, 2019). It is estimated that the global urban population will reach 6.68 billion by 2050, which directly accounts for 68% of the world population (Chen et al., 2022). Obviously, with the continuous development of human society, cities are becoming more and more important homes for human survival (Zhang et al., 2022). The severe high temperature environment poses a huge challenge to the thermal comfort environment of human habitation(Luo et al., 2019; Baruti et al., 2020). Some researches show that >70% of global carbon emissions come from cities(S. Wang et al., 2019). In 2019, China's total carbon emissions accounted for 27.20% of the global total, and the growth rate of carbon emissions was much higher than that of the world's major economies (Tan et al., 2021). From 2000 to 2018, China's total carbon emissions increased by 11.60% annually(Song et al., 2018). The growth of urban carbon emissions has undoubtedly contributed to the deterioration of the urban thermal environment and aggravated the decline of urban living comfort (Zhang et al., 2019; Ren et al., 2019; Kafy et al., 2022).

China's cities are developing rapidly, with the urbanization rate increasing from 18% in 1980 to 64% in 2019, but the land resource consumption is too fast (Jiang et al., 2021). From 2000 to 2018, the area of urban built-up areas increased by 161%, which is twice the growth rate of urban population (81%) in China(Pour, and Najmeh, and Tōnu Oja., 2021). The ever-expanding urban land has brought a series of challenges to the living environment, exacerbating the obvious decline of urban thermal comfort and the rise of carbon emissions(Zhang et al., 2022; Mc Carthy et al., 2018). Especially in the summer urban heat island effect, it is easy to lead to human thermal emergency death and thermal necrosis(Gulcebi et al., 2021). The expansion of urban land is also a great threat to farmland and forest land(Zhang et al., 2022a). Many suburban areas are generated from the conversion of farmland and forest land, which are great damages to local agricultural production and forest land resources(Y. Wang et al., 2020; Miyamoto, 2020). In the process of urbanization, the development of comprehensive land such as commercial areas and factories is generally the main development(Tian et al., 2019). This will generate a lot of carbon emissions, and release a lot of waste heat in the air, thereby exacerbating the greenhouse effect and urban heating effect to a certain extent(Shen et al., 2020). The production of large amounts of greenhouse gases will exacerbate global temperature rise, and will also contribute to the rate of melting of Antarctic glaciers(Levine and Steele, 2021). As a result, some coastal cities are submerged by sea water, which has a negative impact on the sustainable development of urban environment (Echendu, 2020). Scientifically and rationally controlling urban construction and development and moderately slowing down the pace of urban land expansion are crucial to alleviating the pressure on urban thermal environment and carbon emissions (Yang et al., 2020b; Zhang et al., 2022b).

In the direction of urbanization development and human settlements, many scholars have conducted in-depth research. Some scholars believed that urbanization is an important factor in the soaring carbon emissions of buildings(Huo et al., 2020; S. Wang et al., 2018). Relevant studies have revealed that the significant expansion of urban land has led to the reduction of large-scale vegetation cover and the reduction of the carbon-neutral capacity of forests, thereby accelerating carbon emissions, increasing surface temperature and global warming(Dale et al., 2011; Liu et al., 2021). Some studies shown that urbanization development has a destructive impact on biodiversity (Fenoglio et al., 2020; Yang et al., 2020a). As a result, the reduction of biodiversity is accelerated, the imbalance of ecosystems is aggravated, and the instability of human settlements is indirectly promoted (B. Wang and Luo, 2022; Yang et al., 2018). In addition, some studies have found that urbanization will increase carbon emissions in both the long and short term, and there is a one-way short-term causal relationship from urbanization to carbon emissions(Verbić et al., 2021; Joshua et al., 2020). Recently, many scholars have simulated and predicted changes in LULC and LST of cities around machine learning algorithms such as artificial neural network (ANN), including Wuhan in China(Zhang et al., 2022c), Ikom in Nigeria(Mohammad et al., 2022), and Faisalabad in Pakistan(Tariq and Shu, 2020). Abdulla - Al Kafy et al. used machine learning algorithm (MLA) to predict LULC, seasonal (summer and winter) LST and UTFVI changes of Cumilla City Corporation in Bangladesh(Kafy et al., 2021). Yatoo et al. used cellular automata (CA) simulation and ANN to monitor land use change and its future prospects in Ahmedabad, India(Yatoo et al., 2022). Sekertekin et al. used artificial neural network technology to simulate the day and night LST in arid climate regions using Landsat time series data(Tan et al., 2021). Deo and Şahin used ANN algorithm combined with satellite derived surface temperature (LST) to predict long-term global solar radiation in Queensland(Deo and Şahin, 2017).

These studies discussed the impact of urban sprawl on the urban thermal environment from different perspectives, and there is no shortage of studies that continue to explore the relationship between urban sprawl and carbon emissions. However, most of these studies only analyze and discuss one of these directions, and there are few studies discussing the impact of urban expansion on urban thermal environment and carbon emissions. In addition, these studies either discuss the impact of changes in urban sprawl on the thermal environment around single-period or multi-period remote sensing image data, or simply use artificial neural networks to predict changes in urban land use or surface temperature. Few studies have used deep learning to both predict urban land-use change and surface temperature change, and explore the relationship between urban sprawl and the two. It has aroused widespread concern that exploring the relationship between LULC and LST changes and carbon emissions will help cities formulate future sustainable development strategies.

Although the simulation and prediction of future LULC and LST changes is a conventional method, it is a new idea to predict the seasonal (summer and winter) changes of LST using the long short-term memory (LSTM) model of the improved whale optimization algorithm (IWOA). This paper makes a further study on this issue based on previous studies. The artificial neural network-cellular automata (ANN-CA) model is used to predict the changes of LULC in Wuhan, and the IWOA-LSTM is used to predict and analyze the LST in winter and summer. We quantitatively analyze the changes of LULC and LST in different periods, and further explore the correlation between LST and carbon emissions. This study may provide new clues for the prediction of LST in similar regions or cities in the world and the discussion of the relationship between LST and carbon emissions, which can also provide a reference for curbing and reducing the pressure on urban carbon emissions.

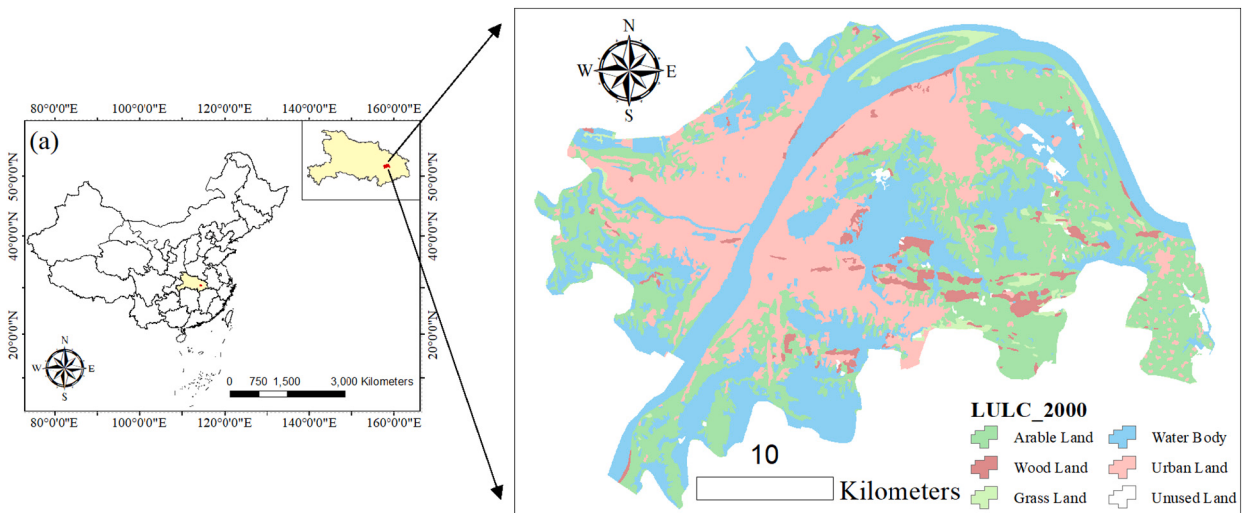


Fig. 1. Location map of the study area.

2. Study area and data sources

2.1. Study area

Wuhan is located in the eastern part of Hubei Province, where the Yangtze River and the Han River meet. It belongs to the north subtropical monsoon humid climate, with abundant rainfall, sufficient sunshine, hot summer and cold winter. The central urban area of Wuhan (Jiang'an District, Jianghan District, Qiaokou District, Hanyang District, Wuchang District, Hongshan District, Qingshan District) is the research area of this paper (Fig. 1). As of the end of 2019, the land area of Wuhan was 8569.15 km², and the built-up area was 812.39 km². Wuhan is located inland of China and far from the ocean. During the early summer rainy season, the rainfall is concentrated, and it is easy to collect heat and dissipate heat. There are many rivers and lakes, which generate a large amount of water vapor at night. Especially during the drought period, the control of subtropical high pressure has a strong urban heat island effect, which is known as one of the “three stoves” cities in China. The annual average temperature is 15.8 °C ~ 17.5 °C, the extreme maximum temperature is 41.3 °C (August 10, 1934), and the extreme minimum temperature is -18.1 °C (January 30, 1977). With the acceleration of urbanization in Wuhan, the social and economic level has also entered a new level. In 2020, the regional GDP will exceed 1.5 trillion yuan, ranking among the top cities in China. As of the end of 2021, the urban permanent population of Wuhan was 11.54 million, accounting for 84.56% of the total population (the urbanization rate of the permanent population), with an increase rate of 0.25% from the end of the previous year. Wuhan's carbon emissions are also rising. By 2022, Wuhan's carbon emissions will basically reach its peak, with carbon emissions reaching 173 million tons. It is one of the first cities to explicitly propose a quantitative target for peak carbon emissions in China.

2.2. Data sources

In this study, the landsat multispectral remote sensing image data are all from the official website of U.S. Geological Survey (<http://earthexplorer.usgs.gov/>). In order to explore the changes of LST in winter and summer in the central urban area of Wuhan, we selected two images in summer (June–July) and winter (December) with cloud cover lower than 10% during the download process. Landsat 4–5 Thematic Mapper (TM) and Landsat 8 Operational Land Imager (OLI) image data were used as research data to monitor LULC changes, LST distribution and correlation indices. Table 1 summarizes all imaging information obtained from the USGS' online data catalog. In this study, ENVI 5.3 was used for image preprocessing. The vector data of Wuhan's administrative divisions are used for the study area division, and the weather station data is used for the temperature verification of the inversion, from the China

Table 1

Description of the collected seasonal satellite image from USGS Earth Explorer.

Date	Sensor	Path/Row	Multi-spectral band resolution	Thermal Band resolution	Cloud Cover
2000/07/27	TM	123/39		120 m (resampled to 30 m)	
2010/06/21	TM	123/39		120 m (resampled to 30 m)	
2020/07/02	OLI	123/39		120 m (resampled to 30 m)	
2000/12/02	TM	123/39	30 m	120 m (resampled to 30 m)	<10%
2010/12/30	TM	123/39		120 m (resampled to 30 m)	
2020/12/25	OLI	123/39		120 m (resampled to 30 m)	

Meteorological Data Network (<http://data.cma.cn/>). In addition, the carbon emission data comes from the Center for Global Environment Research (https://db.cger.nies.go.jp/dataset/ODIAC/DL_odiac2020b.html), which is obtained by mask extraction based on the ArcGIS 10.3 platform.

2.3. LULC classification

In this study, the land use data used comes from Landsat TM remote sensing images, the download address is the Geospatial Data Cloud website (<http://www.gscloud.cn/search>), and the spatial resolution of remote sensing images are 30 m. Images from three different years were collected at closer acquisition dates to avoid seasonal variations in the area. Remote sensing images are classified by ENVI 5.3 software combined with supervised classification and human-computer interaction interpretation. With the help of Google Earth software and field survey methods, the land use data of three phases in 2000, 2010 and 2020 were obtained in the central urban area of Wuhan. The overall accuracy and kappa statistic are used to evaluate the accuracy of LULC classification. We refer to China's "Land Use Status Classification" standard and divide it into six categories: arable land, wood land, grass land, water body, urban land, and unused land (Zhang et al., 2019).

3. Research methods

3.1. Surface temperature inversion

The widely used radiative transfer equation method was selected to perform temperature inversion for the 5th band of the Landsat TM image and the 10th band of the TIRS image. First, the influence of the atmosphere on the surface heat radiation is estimated, and then this part of the atmospheric influence is subtracted from the total heat radiation to obtain the surface heat radiation intensity, which is then converted into the real surface temperature (Wan et al., 2021; Yang et al., 2019). In this paper, the planck function is used for ground temperature extraction, and the formulas are as follows.

$$T_s = K_2 / \ln[K_1 / B(T_s) + 1] \quad (1)$$

$$B(T_s) = [L_\lambda - L^\dagger - \tau(1 - \varepsilon)L_\downarrow] / \tau\varepsilon \quad (2)$$

$$L_\lambda = [\varepsilon B(T_s) + (1 - \varepsilon)L^\dagger] \tau + L^\dagger \quad (3)$$

where the T_s is the surface temperature obtained from the inversion, °C. The $B(T_s)$ is the black body radiance. The ε is the surface specific emissivity. The τ , L^\dagger , L_\downarrow are the atmospheric transmittance, atmospheric upward radiance, and atmospheric downward radiance, respectively, which can be obtained by querying the NASA website. The L_λ is the thermal infrared radiance value, K_1 , K_2 are constants. For TM image: $K_1 = 607.76 \text{ W} \cdot \text{m}^{-2} \cdot \mu\text{m}^{-1} \cdot \text{sr}^{-1}$, $K_2 = 1260.56 \text{ K}$. For OLI image: $K_1 = 774.89 \text{ W} \cdot \text{m}^{-2} \cdot \mu\text{m}^{-1} \cdot \text{sr}^{-1}$, $K_2 = 1321.08 \text{ K}$. The surface specific emissivity is calculated by the pixel binary model based on the surface coverage type (Al-Hemoud et al., 2019), and the formulas are as follows:

$$\varepsilon = 0.004F_v + 0.986 \quad (4)$$

$$F_v = (I_{\text{NDVI}} - I_{\text{NDVI,soil}}) / (I_{\text{NDVI,veg}} - I_{\text{NDVI,soil}}) \quad (5)$$

where NDVI is the normalized vegetation index, F_v is the vegetation coverage. NDVI_{veg} and NDVI_{soil} generally take the maximum and minimum values of a certain confidence interval. Referring to the previous research results, the cumulative percentage of 5% and 95% was used as the confidence interval, and the empirical value was used to obtain $I_{\text{NDVI,veg}} = 0.05$, $I_{\text{NDVI,soil}} = 0.7$. That is, when the I_{NDVI} of a pixel is >0.7 , the F_v value is 1; when the I_{NDVI} is <0.05 , the F_v value is 0.

3.2. Artificial neural network-cellular automata model (ANN-CA)

This paper uses the ANN-CA model to forecast the LULC of Wuhan in 2030 and 2040 based on the LULC data of 2000, 2010 and 2020. The cellular automata in the ANN-CA model consists of four parts, and the CA model is described in the language of the set (Rahman and Esha, 2020). The formula is as follows.

$$W_{t+1} = \psi(W_t, N) \quad (6)$$

where the W_{t+1} is LULC of Wuhan in 2030 and 2040, W_t is the LULC of Wuhan in 2020. N is the cell neighbourhood; ψ is the conversion rule. The CA cells are discretely distributed in a multi-dimensional space. We use the conversion probability between different erosion levels obtained by the ANN as the conversion rule of the CA to realize the coupling between the two, reducing the difficulty of defining rules and avoiding the influence of human subjective factors (Sarkar et al., 2021).

The ANN-CA model adopts the BP neural network (BPNN), which is widely used at present. BPNN can dynamically adjust the weight of each neuron connection in the network according to the error, gradually reduce the network error, and finally obtain an ideal network model (Abbas et al., 2021). The BPNN consists of input layer, hidden layer, and output layer. The neurons in the input layer

are the main factors affecting soil erosion changes and determine the erosion level transition probability of the cells at time t . The output layer neurons represent the target state of the cell. The input layer of this paper is LULC in 2010 and 2020, elevation data, road data, night light data soil type data, and population data. The output layer is 2030 LULC(Baig et al., 2022). The conversion probability calculation formula is as follows:

$$Q(j, t, l) = 1 + (-\ln \gamma)^{\beta} \sum_k \omega_{k,l} \frac{1}{1 + e^{-net_k(j,t)}} \quad (7)$$

In the formula: $Q(j, t, l)$ is the transition probability of the state of cell j from time t to the next time. $\omega_{k,l}$ is the weight value between the hidden layer and the output layer. $\frac{1}{1+e^{-net_k(j,t)}}$ is the response value of the hidden layer. γ is a random number between [0,1], and β is a random interference intensity parameter.

3.3. Long short-term memory (LSTM)

With the continuous improvement and development of deep learning theory, the concept of time series is introduced, which not only pays attention to the processing of information at the current moment, but also realizes the connection of time information before and after, thereby improving the accuracy of analysis. For example, the recurrent neural network (RNN) introduces this concept into network construction, and its essential feature is that there are both internal feedback connections and feedforward connections between the processing units of the network layer. The model can perceive information from multiple time perspectives. Compared with the RNN model, the LSTM has better performance in longer sequences, mainly to solve the problems of gradient disappearance and gradient explosion during training of long sequences. This is helpful in LST prediction, it can reduce over-fitting and loss of prediction information and accuracy in the prediction process. LSTM introduces the cell state to memorize information, and adds three gates (input gate, forget gate, output gate) structure to realize the protection and control of LST(Le, and Lee, and Jung., 2019; Sherstinsky, 2020). The main formulas are expressed as follows.

$$\text{Input gate : } j_t = \delta(W_i \cdot [m_{t-1}, l_t] + a_i) \quad (8)$$

$$\text{Forget gate : } k_t = \delta(W_f \cdot [m_{t-1}, l_t] + a_f) \quad (9)$$

$$\tilde{C}_t = \tanh(W_c \cdot [m_{t-1}, l_t] + a_c) \quad (10)$$

$$\text{Output gate : } P_t = \delta(W_o \cdot [m_{t-1}, l_t] + a_o) \quad (11)$$

$$\text{Long memory : } C_t = f_t \times C_{t-1} + j_t \times \tilde{C}_t \quad (12)$$

$$\text{Short memory : } h_t = P_t \times \tanh(C_t) \quad (13)$$

where l, m are the input vector and output vector of LSTM, respectively; k is the forget gate, j is the input gate, p is the output gate; C is the unit state of the LSTM neural network; δ, \tanh are the activations of sigmoid and \tanh , respectively function; W and a denote the weight and bias matrices, respectively.

3.4. Whale Optimization Algorithm (WOA)

Aljarah et al. proposed the WOA algorithm, which has simple principle, few parameter settings and strong optimization performance (Gharehchopogh and Gholizadeh, 2019). The model generally divided into three steps: one of the largest baleen whales in the world is the humpback whale, and the most interesting thing about humpback whales is their bubble net foraging method. Using the algorithm optimization of WOA, we divide it into three steps: LST area search, determine the LST optimal solution threshold, and find the LST optimal solution. Using the rule can correct the shortcomings of the long sequence model LSTM and improve the accuracy of LST prediction (Mirjalili and Lewis, 2016; Bozorgi, and Seyed, and Samaneh Yazdani., 2019). The basic formulas of the algorithm are as follows.

$$\text{LST range search : } \vec{A} = \left| \vec{B} \cdot \vec{C} \times (t) - \vec{C}(t) \right| \quad (14)$$

$$\vec{C}(t+1) = \vec{C} \times (t) - \vec{E} \cdot \vec{A} \quad (15)$$

$$\vec{E} = 2 \vec{a} \cdot \text{rand} - \vec{a} \quad (16)$$

$$\vec{B} = 2 \cdot \text{rand} \quad (17)$$

$$a = \left(2 - \frac{2t}{T_{max}} \right) \quad (18)$$

In the formula: $\vec{C} \times (t)$, $\vec{C}(t)$ represents the optimal solution of LST and the range of LST search thresholds; $\vec{E} \cdot \vec{A}$, t is the encircling step size and the current number of iterations, respectively; T_{max} represents the maximum number of iterations; $rand$ represents a random number between [0,1], \vec{a} represents the convergence factor, which linearly decreases from 2 to 0 with the increase of the number of iterations(Rana et al., 2020).

Determine the LST optimal solution threshold:

$$\vec{C}(t+1) = \vec{A}^l \cdot e^{bl} \cdot (\cos 2\pi l) + \vec{C} \times (t) \quad (19)$$

In the formula: \vec{A}^l represents the distance between the $i - th$ search range of the current optimal LST. b is the constant coefficient used to define the logarithmic spiral form; l represents the randomness between [-1,1] number(Kaveh and Ilchi Ghazaan, 2017).

Searching for the optimal solution of LST:

$$\vec{A} = \left| \vec{B} \cdot \vec{c}_{rand}(t) - \vec{C}(t) \right| \quad (20)$$

$$\vec{C}(t+1) = \vec{c}_{rand}(t) - \vec{E} \cdot \vec{A} \quad (21)$$

In the formula: $\vec{c}_{rand}(t)$ represents the position vector of randomly selected LST.

3.5. Improved whale optimization algorithm (IWOA)

The whale optimization algorithm has good optimization ability, and the most obvious advantage is its global convergence ability and fast convergence speed. However, when using WOA to update the cell weight matrix, because the optimization area is too large, the WOA optimization accuracy in the later stage of training is poor and the weight convergence speed is too small (Yang et al., 2020a). Due to the traditional WOA algorithm is easy to fall into the local optimum, the optimization accuracy is low and the convergence speed is slow. Therefore, we use the improved WOA algorithm to predict LST, and uses chaos to initialize the population to ensure the diversity of the initial population. The chaotic map has a simple structure, and it can be used to mutate the current optimal individual to generate a new individual, which can quickly search for the LST global optimal solution(Xiong et al., 2018; H. Zhang et al., 2019). In the actual LST prediction range, the early search LST range is relatively large, and it is necessary to quickly search and locate the area range of the LST. In the later stage, it is necessary to finely search for the LST optimal solution. When the distance to the LST optimal solution is close, the step size is too large and it is easy to fall into the local optimal prematurely. The standard whale algorithm convergence factor decreases linearly from 2 to 0, but the linearly decreasing convergence factor cannot well distinguish the global search of LST from the local search of LST. Therefore, this paper improves the decreasing form of the convergence factor (a) in the traditional whale algorithm, and changes the linear decreasing method to the nonlinear decreasing method (Butti et al., 2020). The specific formulas are as follows.

$$K_{n+1} = \begin{cases} \frac{K_n}{q}, & 0 < K_n \leq q \\ \frac{1-K_n}{1-q}, & q < K_n < 1 \end{cases} \quad (22)$$

Where the parameters $K_n \in (0,1)$, $q \in (0,1)$.

3.6. LSTM model based on IWOA (IWOA-LSTM)

The adaptive moment (Adam) optimizer of the traditional LSTM model has a momentum term, so it can speed up the training speed of the LSTM, but it is also easy to cause the LSTM to fall into a local minimum, the accuracy of short-term prediction is not high, and the goodness of fit is poor. In view of the above problems, this paper combines the Adam optimizer in LSTM, inherits the momentum term of the Adam optimizer in LSTM, and makes it have a momentum-driven function, and then optimizes the weight search area efficiently. It will further reduce and avoid the prediction bias of the LSTM model due to human experience differences. This paper uses the improved WOA to LSTM to forecast the LST in the central urban area of Wuhan in 2030 and 2040. The number of iterations of the WOA algorithm model, the learning rate, the neurons in the first hidden layer, and the neurons in the second hidden layer are optimized. The improved model can predict LST in the short term and quickly select the optimal interval of LST, which shows that IWOA-LSTM has better effect than LSTM model(Xu et al., 2022).

4. Results and analysis

4.1. LULC classification and prediction

In this study, based on the support vector machine (SVM) under ENVI5.3 software, LULC classification is performed on the remote sensing images of Wuhan in 2000, 2010 and 2020 (Fig. 2a, b and c). In addition, the classification results show that the overall accuracy rate and the percentage of Kappa coefficient of Wuhan's LULC classification map in 2000, 2010 and 2020 are 89.33%, 86.26%,

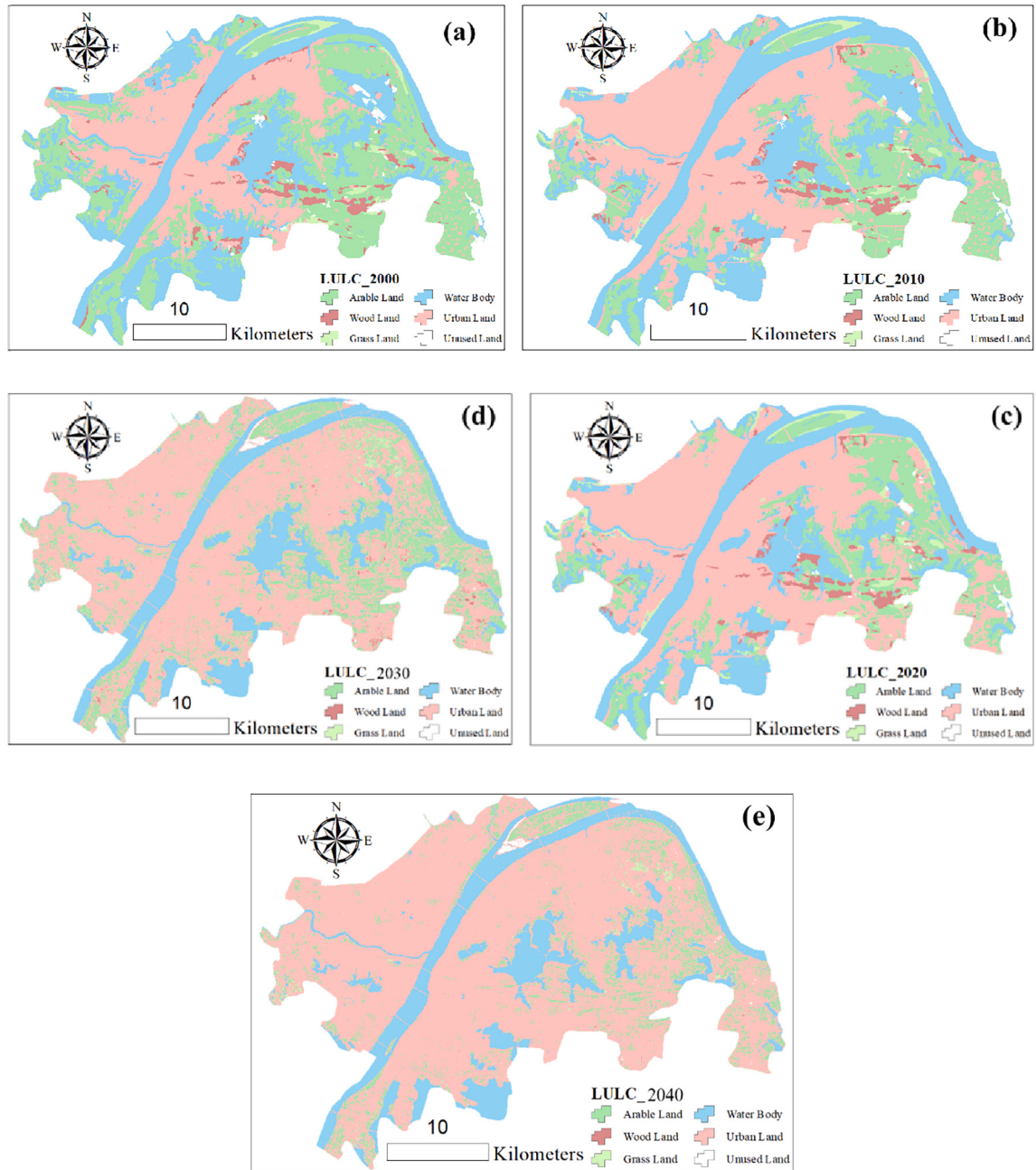


Fig. 2. The map of the LULC classification and prediction.

85.66% and 90.52%, 88.31% and 87.34% respectively, indicating that the classification accuracy rate is high. From Fig. 2a, b and c, we find that urban land in the central urban area of Wuhan has grown rapidly, showing a trend of expanding from the center to the surrounding areas. In addition, based on the ANN-CA model, we forecast the central urban area in 2030 and 2040. First, we use the LULC data of 2000 and 2010 to predict the change of LULC in 2020, and compare the LULC simulated by ANN-CA model in 2020 with the actual LULC in 2020 in the QGIS v2.18 platform to verify the accuracy of the simulated LULC. The results show that the predicted Correctness of LULC in Wuhan in 2020 reaches 89.69%, and the Kappa (overall) is 0.81, indicating that the model has a good statistical accuracy, and the model is suitable for predicting the future LULC. Therefore, we can simulate the LULC changes in 2030 and 2040 based on the ANN-CA model (Fig. 2d and e).

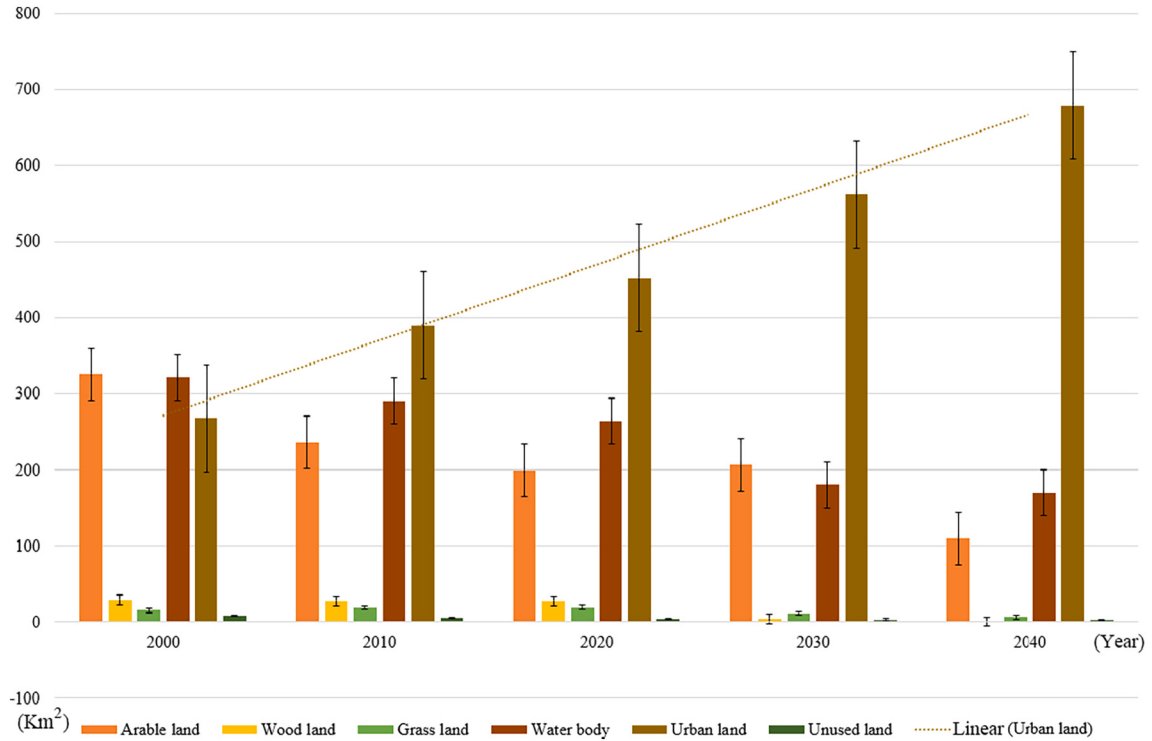


Fig. 3. Statistics of LULC changes.

4.2. LULC change analysis

We counted the area changes of various land use types of Wuhan in 2000, 2010, 2020, 2030 and 2040 (Fig. 3). Fig. 3 shows that from 2000 to 2040, Wuhan's urban land use showed a trend of accelerated expansion, with a high growth rate. The area of urban land will increase from 268.149 km^2 in 2000 to 678.932 km^2 in 2040, with an increase rate of 60.50%. The other five types of land areas all showed varying degrees of reduction. The land type with the largest reduction in the area of various land use types is forest land, which will decrease from 29.630 km^2 in 2000 to 0.390 km^2 in 2040, with a reduction rate of 98.68%. The land type with the least area reduction is water body, and the reduction rate of water body area from 2000 to 2040 is 47.02%. The reduction rates of grassland, cultivated land and unused land area are 57.74%, 66.37% and 60.25%, respectively.

4.3. Winter and summer LST inversion distribution and prediction analysis

With the land surface inversion method in the section 3.1, we have retrieved the winter and summer surface temperature of Wuhan in 2000, 2010 and 2020. The Figs. 4.1a, b, c and 4.2a, b and c reveal that the temperature in the central urban area from 2000 to 2040 has risen to varying degrees in winter and summer, and the area covered by the high temperature layer has an obvious trend of expansion. In addition, we forecast the temperature in winter and summer in 2030 and 2040 based on the IWOA-LSTM model. First, we established a 100×100 fishing net to extract the LST distribution results, and then performed the 2020 forecast analysis on the extracted 2000 and 2010 data. The R^2 of the prediction result is 91.31%, indicating that the prediction result is accurate. The prediction results of winter and summer are shown in Figures 4.1d, e and 4.2d, e. These figures reveal that the high-temperature layer shows a significant expansion trend, especially in the areas where the temperature is higher than 15°C in winter and higher than 30°C in summer in Wuhan.

4.4. Analysis of the variation trend of LST in winter and summer

According to the forecast results from 2000 to 2040, the changes of LST in winter and summer are statistically shown in Fig. 5. Fig. 5a shows that the most significant expansion and growth of winter temperature is in the temperature range of $10^\circ\text{C} \sim 15^\circ\text{C}$, which increases by 93.64% from 2000 to 2040. The regional expansion above 15°C is also significant, which will increase from 0.002 km^2 in 2000 to 1.027 km^2 in 2040 in winter. Moreover, the area in the temperature range of $<2.5^\circ\text{C}$ and $2.5^\circ\text{C} \sim 5^\circ\text{C}$ will be zero in 2040, and the area in the temperature range of $5^\circ\text{C} \sim 10^\circ\text{C}$ will be reduced by 62.52% from 2000 to 2040.

Fig. 5b shows that the temperature in Wuhan has a significant upward trend in summer, with the area of low temperature shrinking and the area of high temperature expanding. The area in the temperature range of $23^\circ\text{C} \sim 25^\circ\text{C}$ decreased the most, and the area in

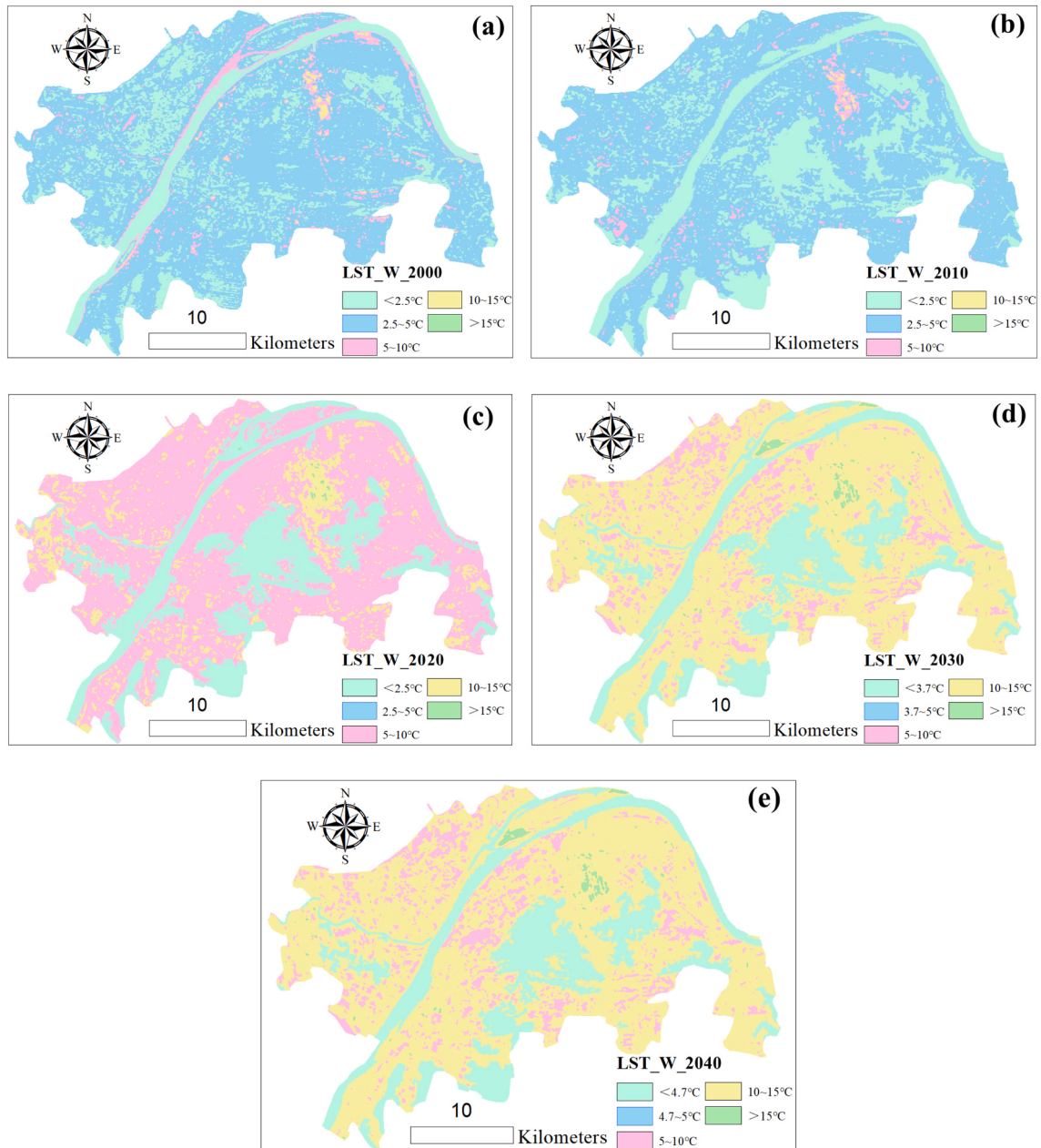


Fig. 4.1. The map of LST distribution and forecast in winter.

Fig. 4.2 The map of LST distribution and forecast in summer.

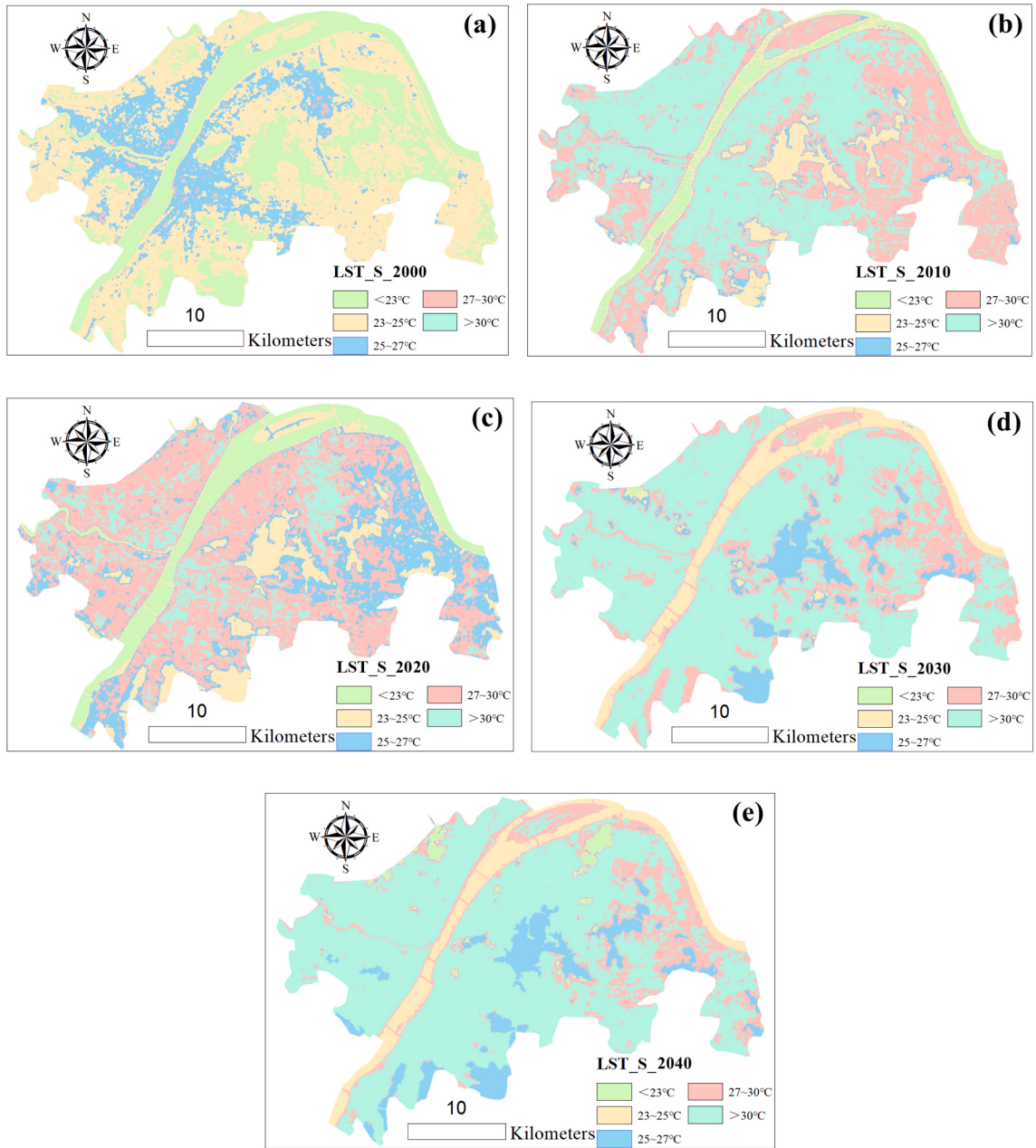


Fig. 4.1. (continued).

this range decreased by 95.86% from 2000 to 2040. During the study period, the second obvious contraction of the temperature area was the temperature range $<23^{\circ}\text{C}$, and the area decreased by 95.41%. However, the area with a temperature range of $>30^{\circ}\text{C}$ shows obvious expansion characteristics. The temperature range expands from 0.045 km^2 in 2000 to 657.516 km^2 in 2040. The area in the temperature range of $27^{\circ}\text{C} \sim 30^{\circ}\text{C}$ will expand from 8.612 km^2 in 2000 to 203.942 km^2 in 2040.

4.5. LST distribution under different LULC types

In ArcGIS 10.3 software, the proportions of different types of LULCs in different LST intervals can be obtained (Fig. 6). Fig. 6a and b show that the low temperature area in Wuhan in winter is mainly distributed in water body, which is concentrated in the temperature range of $<2.5^{\circ}\text{C}$ and $2.5^{\circ}\text{C} \sim 5^{\circ}\text{C}$. In 2000, the areas of the water body in these two temperature ranges were 126.905 km^2 and 194.258 km^2 . In 2010, their areas were 117.492 km^2 and 406.993 km^2 , respectively. Fig. 6c shows that the temperature ranges of $5^{\circ}\text{C} \sim 10^{\circ}\text{C}$ and $10^{\circ}\text{C} \sim 15^{\circ}\text{C}$ in winter are mainly concentrated in Arable land and Grassland, and their areas are 247.181 km^2 and

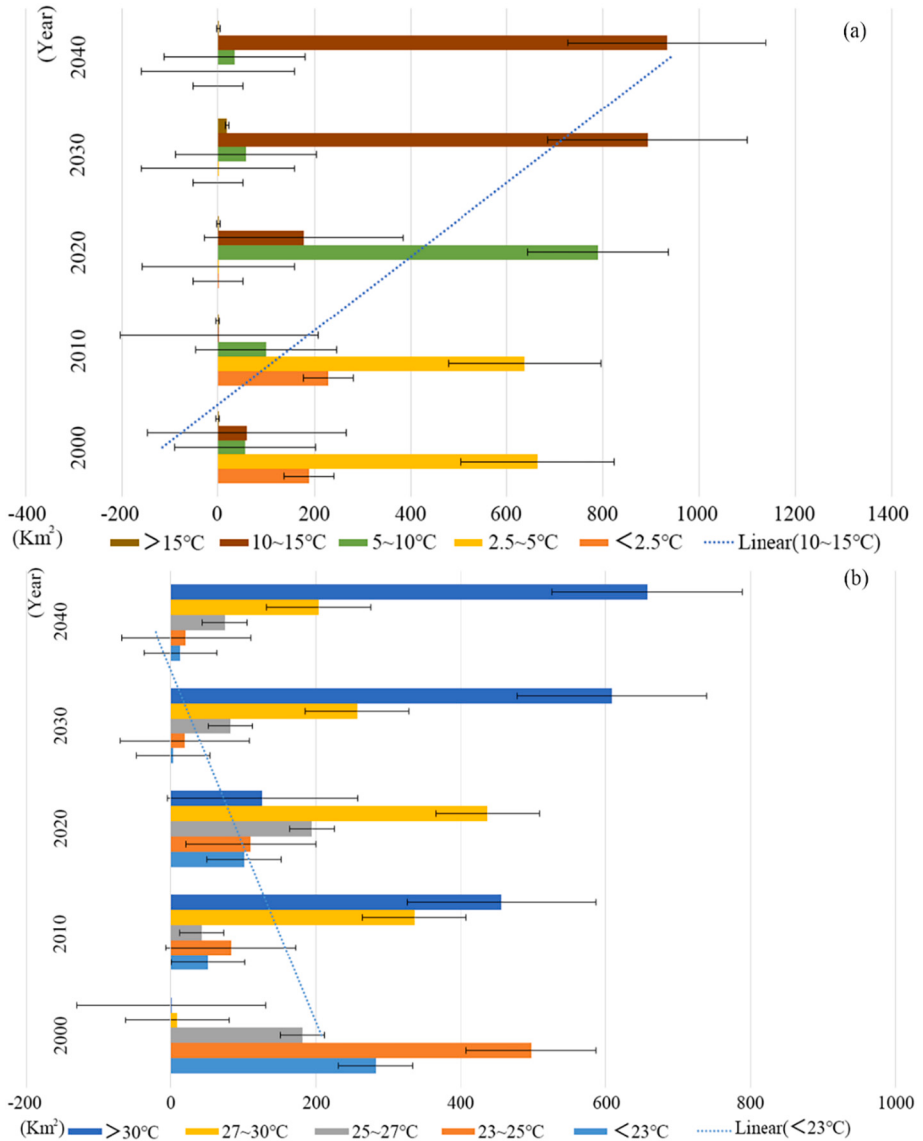


Fig. 5. Change trend of LST in winter and summer.

374.356 km². Fig. 6d and e show that Wuhan's winter high temperature area will expand to urban land in 2030 and 2040. In 2030, the area of the central urban area will be 532.504 km² and 14.336 km² respectively in the temperature range of 10 °C ~ 15 °C and >15 °C. By 2040, the area between 5 °C ~ 10 °C and 10 °C ~ 15 °C will be 243.062 km² and 527.440 km², respectively.

Fig. 7 shows that urban land is the main land use type in the high temperature area in summer, and the temperature of this land use type shows a rising trend with time. Fig. 7b, c, d and e further reveal that urban land has been expanding in the high-temperature area (LST > 27 °C), from 329.455 km² in 2010 to 573.956 km² in 2040, with an increase rate of 42.60%. In addition, the land type mainly concentrated in the low temperature area (LST < 23 °C) in summer is water body. However, the overall surface temperature of Wuhan is rising, and the area of the low temperature zone in the water body is shrinking from 2030 to 2040. The area of the water body in the low temperature area decreased from 211.329 km² in 2000 to 0.836 km² in 2040. The area of the low temperature region (LST < 23 °C) of arable land, wood land and grass land also decreased to varying degrees.

4.6. Analysis of the characteristics of carbon emissions in winter and summer

We selected the monthly average carbon emission data in winter and summer for seasonal analysis (Fig. 8). Fig. 8a, c and e are the carbon emission distribution maps of Wuhan in winter in 2000, 2010 and 2020, respectively, and Fig. 8b, d and f are the corresponding summer carbon emissions distribution maps. These figures show that the carbon emissions in Wuhan are increasing both in winter and summer. From 2000 to 2020, the carbon emissions increased by 67.68% in winter and 67.35% in summer. However, in the three years,



Fig. 6. LST distribution of different types of LULC in winter.

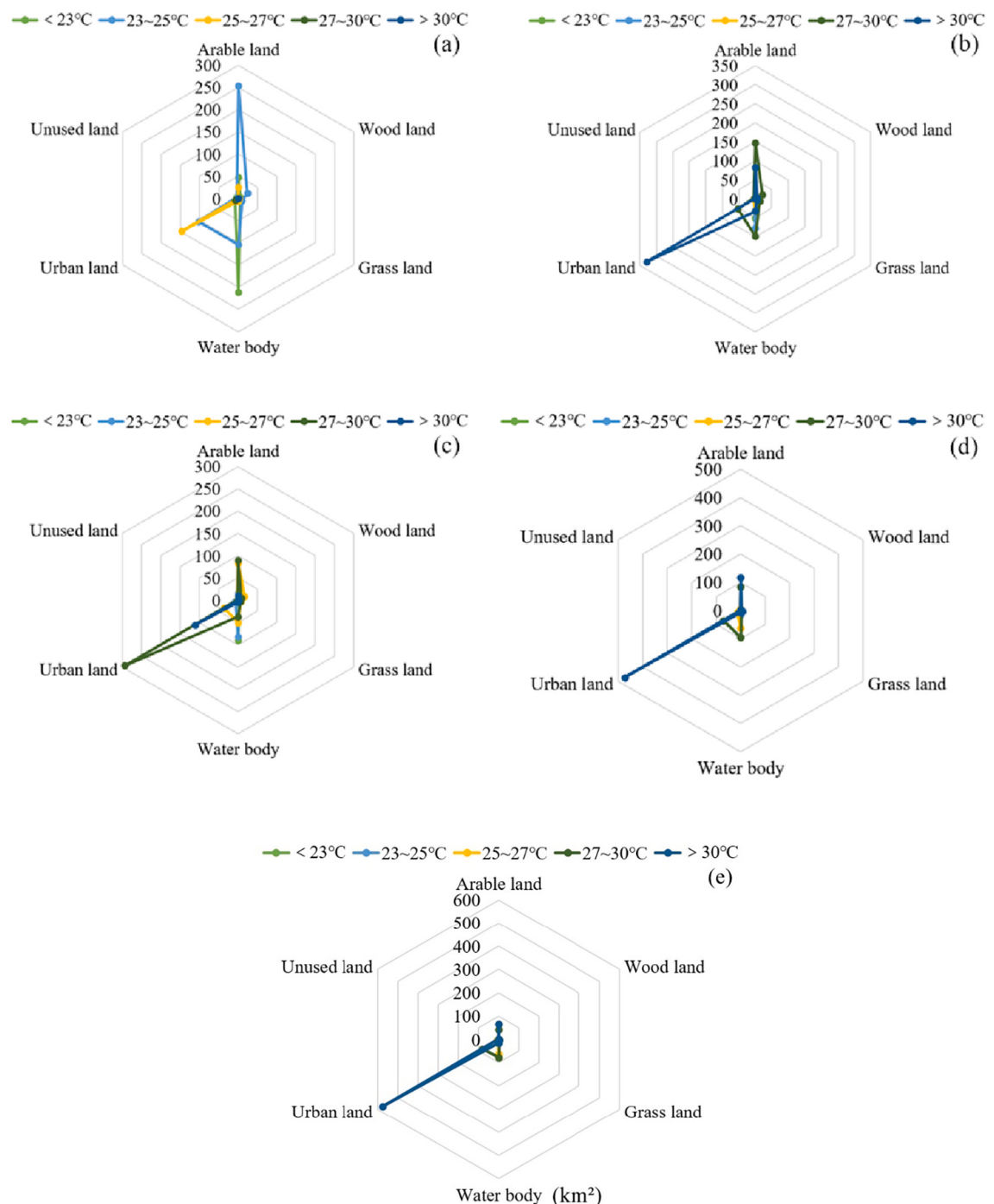


Fig. 7. LST distribution of different LULC types in summer.

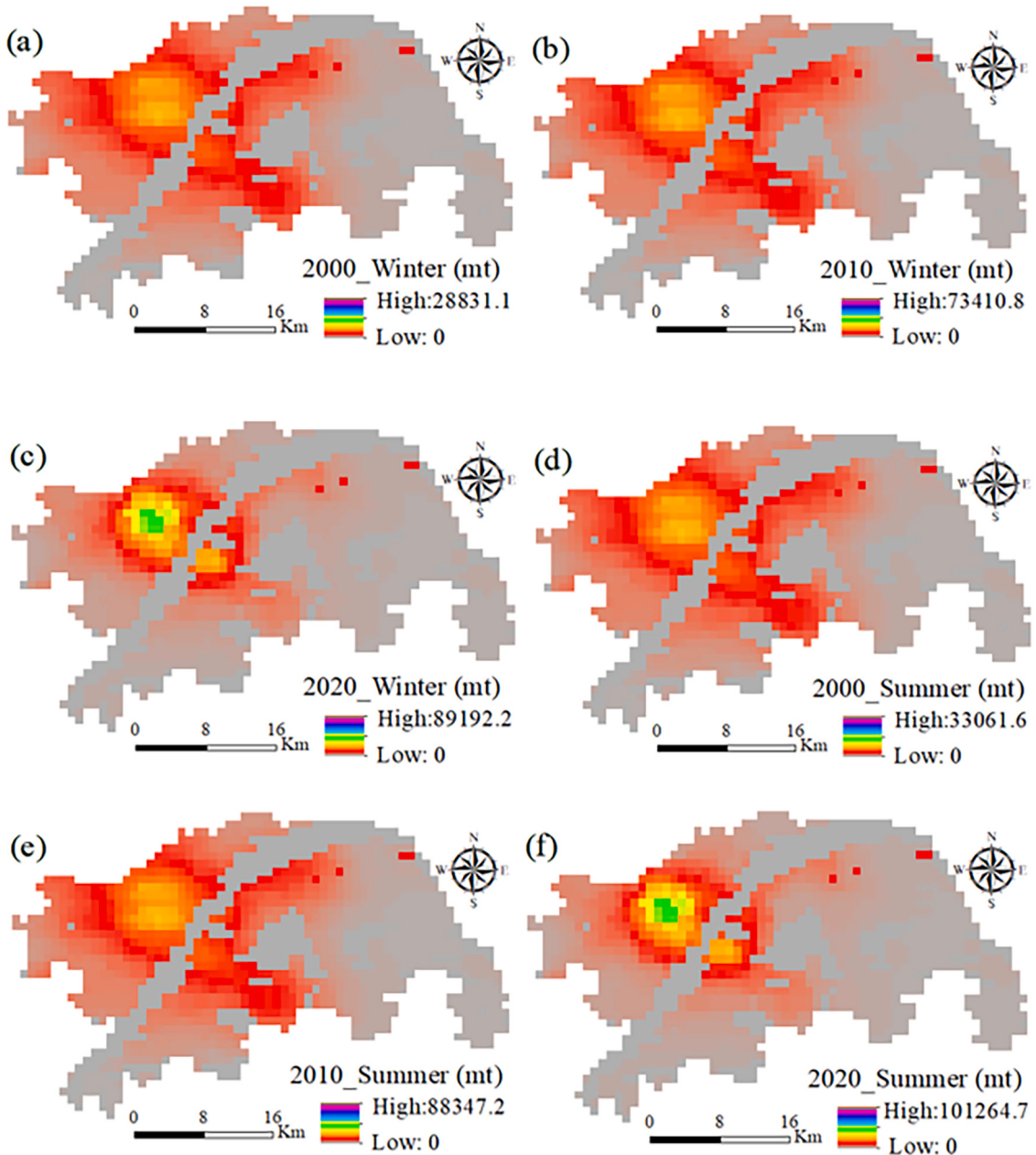


Fig. 8. Distribution of carbon emissions.

Wuhan's carbon emissions in summer are generally higher than those in winter. In 2000, the highest carbon emission was 33,061.6 mt in summer and 28,831.1 mt in winter. In 2020, Wuhan's carbon emissions increased greatly in winter and summer, with the highest carbon emissions reaching 101,264.7 mt in summer and 89,192.2 mt in winter. This may be due to the high temperature weather in Wuhan in summer, which increases the carbon emissions of refrigeration equipment such as air conditioners.

4.7. Analysis of the relationship between carbon emissions and LST

In ArcGIS V10.3 platform, we use 100 * 100 fishing nets to extract multiple values of LST and carbon emission layers and perform correlation fitting analysis (Fig. 9). Fig. 9a, c and e are the correlation fittings of carbon emissions and LST in winter, and 9b, 9d and 9f are the fittings of carbon emissions and LST in summer. These figures reveal a clear correlation between carbon emissions and LST changes. In summer and winter of 2000, the R^2 of linear fitting between LST and carbon emissions was low, 0.6227 and 0.6143

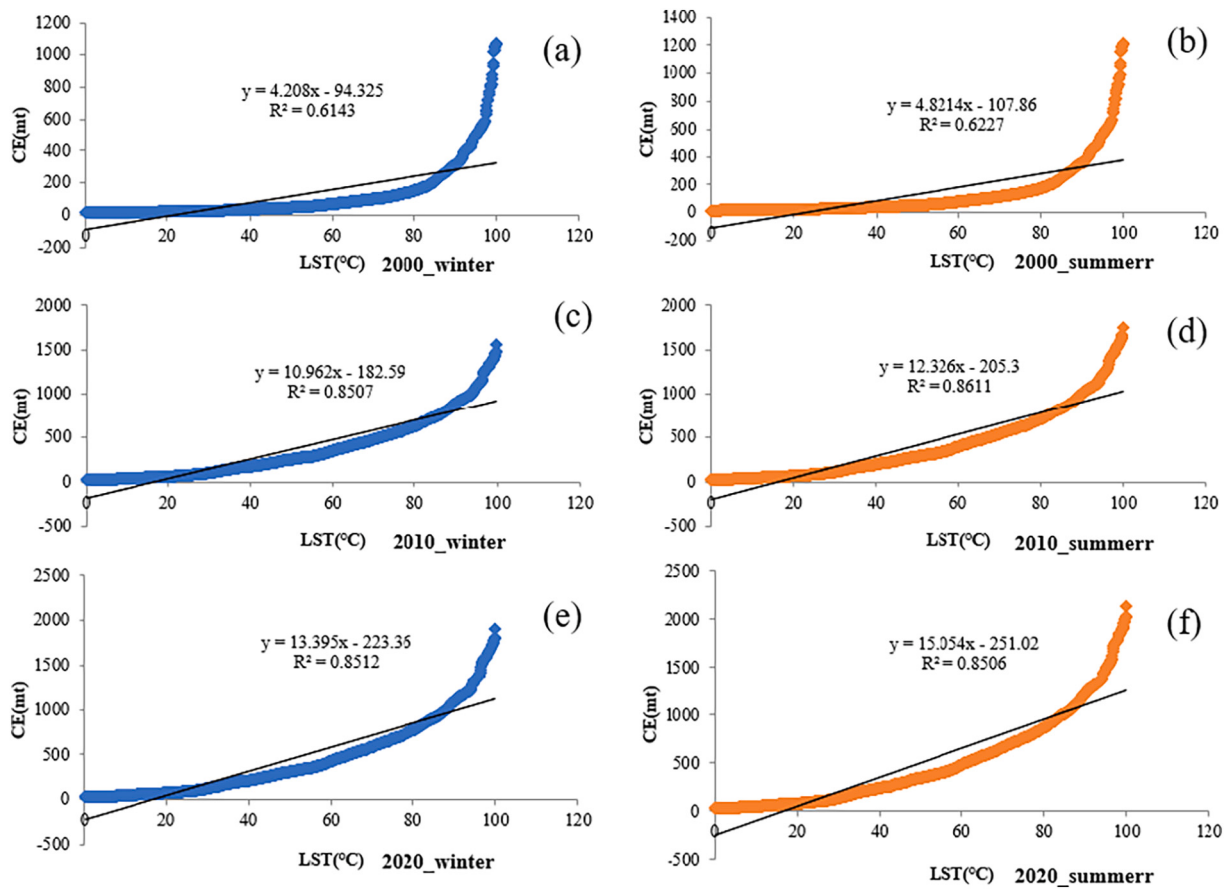


Fig. 9. Fitting chart of correlation between carbon emissions and LST.

respectively. In 2010 and 2020, the R^2 of linear fitting is higher than 0.85 no matter in winter or summer. This shows that the carbon emissions have obvious correlation with LST of Wuhan, and the correlation fluctuation is low from 2010 to 2020.

5. Conclusions and discussions

5.1. Conclusions

Based on the LULC, LST and carbon emission data of Wuhan in 2000, 2010 and 2020, this paper discusses the impact of LULC on LST and carbon emissions in winter and summer using the ANN-CA, IWOA-LSTM and linear models. The work shows that with the rapid progress of urbanization, urban land will continue to expand, and the area of other land use types will be reduced without reasonable control of the scale of urban land. The high temperature area of urban land is continuing to expand, while the green space and water body in the low temperature area are gradually shrinking (Huang et al., 2019). This inevitably exacerbates the rise of LST in the central urban area and reduces the comfort of the urban environment (Abir and Saha, 2021).

In addition, based on the IWOA-LSTM model, the LST in winter and summer is predicted in 2030 and 2040. We found that the area of high temperature ($LST > 27^\circ\text{C}$) is expanding continuously. In summer, the area with $LST > 30^\circ\text{C}$ accounts for $>67.84\%$ of the total area, and the area with $LST > 10^\circ\text{C} \sim 15^\circ\text{C}$ accounts for $>96.32\%$ of the total area in winter. Urban land occupies a relatively high area in the high temperature range in both winter and summer, with winter accounting for 54.42% and summer accounting for 59.22%. The expansion of urban land in the central urban area of Wuhan has a significant stimulating effect on the rise of LST, but the impact of urban land on LST is more significant in summer than in winter.

Finally, during the study period, the carbon emissions in the central urban area of Wuhan will continue to increase without taking positive measures. The linear fitting results of carbon emissions and LST show that there is a strong correlation between carbon emissions and LST. The R^2 of linear fitting between LST and carbon emissions in summer and winter of 2000 were 0.6227 and 0.6143 respectively. The R^2 of linear fitting in summer and winter is higher, both of which are >0.85 in 2010 and 2020. The above analysis can provide guidance for urban planning and construction, and provide decision support for the low-carbon and green development of cities, as well as provide a more microscopic control mechanism for the rational construction of cities.

5.2. Discussions

With the continuous expansion of urban land in the central urban area of Wuhan, the LST in both winter and summer has increased significantly, and the expansion of high-temperature areas of urban land has accelerated, while the low-temperature areas of water bodies and green land have shrunk significantly. It should be noted that the urban land still shows an obvious expansion trend, with its area increasing from 268.149 km² in 2000 to 678.932 km² in 2040. Moreover, carbon emissions show an obvious growth trend, and the growth rate in summer is significantly higher than that in winter. The linear fitting results between LST and carbon emissions show that there is a strong correlation between LST and carbon emissions. It may be mainly due to the rapid progress of urbanization, which has led to the rapid growth of the impervious area of the city, the expansion of the flow of people and vehicles, and the rising energy consumption, which indirectly promoted the increase of LST and carbon dioxide emissions. This kind of development mode that only considers the rapid expansion of cities is deformed, and more attention should be paid to the quality of urban development and environmental sustainability. It is necessary to attach importance to urban environmental planning and upgrading projects, and control the excessive expansion of urban construction land(Guler and Yomraliooglu, 2021). The unreasonable development land in the central city shall be covered with green construction, and the illegal buildings shall be appropriately demolished to increase the green coverage and increase the green coverage of the city to slow down and control the rise of LST and carbon emissions.

This paper uses machine learning and geostatistics methods to predict urban land expansion in Wuhan, and explores the impact of future urban expansion on LST, as well as the correlation between LST and carbon emissions. It may provide new clues for future urban development and environmental governance and mitigation of carbon emissions, but the article also has some shortcomings. The IWOA-LSTM model was used to predict the LST changes in Wuhan in 2030 and 2040, but it does not mean that the model is necessarily suitable for other regions. In future research, we need to further discuss other more general models to improve the prediction accuracy. In addition, the resolution of the carbon emission data we use is not high, and there may be a certain bias in the correlation detection of LST. Therefore, further use of higher-precision carbon emission data in future research may be a new direction, which can provide more accurate and objective observations and references for new research.

CRediT authorship contribution statement

Maomao Zhang: Conceptualization, Methodology, Formal analysis, Writing – original draft, Writing – review & editing. **Abdulla - Al Kafy:** Methodology, Writing – review & editing. **Pengnan Xiao:** Writing – review & editing. **Siyu Han:** Writing – review & editing. **Shangjun Zou:** Writing – review & editing. **Milan Saha:** Methodology. **Cheng Zhang:** Methodology, Writing – review & editing. **Shukui Tan:** Supervision.

Declaration of Competing Interest

The authors declare that they have no known competing financial interests or personal relationships that could have appeared to influence the work reported in this paper.

Data availability

Data will be made available on request.

Acknowledgements

The authors would like to thank the reviewers for their expertise and valuable input. This research is funded by the Fundamental Research Funds for the Central Universities (YCJJ202204009).

References

- Abbas, Zaheer, Yang, Guang, Zhong, Yuanjun, Zhao, Yaolong, 2021. Spatiotemporal change analysis and future scenario of LULC using the CA-ANN approach: a case study of the Greater Bay Area, China. Land 10 (6), 584. <https://doi.org/10.3390/land10060584>.
- Abir, Farhan Asaf, Saha, Ritu, 2021. Assessment of land surface temperature and land cover variability during winter: a spatio-temporal analysis of Pabna municipality in Bangladesh. Environ. Challeng. 4 (August), 100167 <https://doi.org/10.1016/j.envc.2021.100167>.
- Al-Hemoud, Ali, Al-Sudairawi, Mane, Al-Rashidi, Mufreh, Behbehani, Weam, Al-Khayat, Ahmed, 2019. Temperature inversion and mixing height: critical indicators for air pollution in hot arid climate. Nat. Hazards 97 (1), 139–155. <https://doi.org/10.1007/s11069-019-03631-2>.
- Baig, Mohammed Feras, Mustafa, Muhammad Raza Ul, Baig, Imran, Takaijudin, Husna Binti, Zeshan, Mohammad Talha, 2022. Assessment of land use land cover changes and future predictions using CA-ANN simulation for Selangor, Malaysia. Water 14 (3), 402. <https://doi.org/10.3390/w14030402>.
- Baruti, Modest Maurus, Johansson, Erik, Yahia, Moohammed Wasim, 2020. Urbanites' outdoor thermal comfort in the informal urban fabric of warm-humid Dar Es Salaam, Tanzania. Sustain. Cities Soc. 62 (November), 102380 <https://doi.org/10.1016/j.scs.2020.102380>.
- Bozorgi, Mostafa, Seyed, and Samaneh Yazdani, 2019. IWOA: an improved whale optimization algorithm for optimization problems. J. Comput. Des. Eng. 6 (3), 243–259. <https://doi.org/10.1016/j.jcde.2019.02.002>.
- Butti, Dasu, Mangipudi, Siva Kumar, Rayapudi, Srinivasa Rao, 2020. An improved whale optimization algorithm for the design of multi-machine power system stabilizer. Int. Trans. Electric. Energy Syst. 30 (5) <https://doi.org/10.1002/2050-7038.12314>.
- Carthy, Mc, Ultan, Ismail Uysal, Badia-Melis, Ricardo, Mercier, Samuel, O'Donnell, Colm, Ktenioudaki, Anastasia, 2018. Global food security – issues, challenges and technological solutions. Trends Food Sci. Technol. 77 (July), 11–20. <https://doi.org/10.1016/j.tifs.2018.05.002>.
- Chen, Mingxing, Chen, Liangkan, Li, Yang, Xian, Yue, 2022. Developing computable sustainable urbanization science: interdisciplinary perspective. Comput. Urb. Sci. 2 (1), 17. <https://doi.org/10.1007/s43762-022-00048-9>.

- Dale, Virginia H., Efroyimson, Rebecca A., Kline, Keith L., 2011. The land use–climate change–energy nexus. *Landsc. Ecol.* 26 (6), 755–773. <https://doi.org/10.1007/s10980-011-9606-2>.
- Deo, Ravinesh C., Şahin, Mehmet, 2017. Forecasting long-term global solar radiation with an ANN algorithm coupled with satellite-derived (MODIS) land surface temperature (LST) for regional locations in Queensland. *Renew. Sust. Energ. Rev.* 72 (May), 828–848. <https://doi.org/10.1016/j.rser.2017.01.114>.
- Echendu, Adaku Jane, 2020. The impact of flooding on Nigeria's sustainable development goals (SDGs). *Ecosyst. Health Sustain.* 6 (1), 1791735. <https://doi.org/10.1080/20964129.2020.1791735>.
- Fenoglio, María Silvina, Rossetti, Marfa Rosa, Videla, Martín, 2020. “Negative Effects of urbanization on terrestrial arthropod communities: a meta-analysis.” edited by Andres Baselga. *Glob. Ecol. Biogeogr.* 29 (8), 1412–1429. <https://doi.org/10.1111/geb.13107>.
- Fu, Jiacheng, Wang, Yupeng, Zhou, Dian, Cao, Shi-Jie, 2022. Impact of urban park design on microclimate in cold regions using newly developed prediction method. *Sustain. Cities Soc.* 80 (May), 103781 <https://doi.org/10.1016/j.scs.2022.103781>.
- Gao, Kang, Yuan, Yijun, 2022. Is the sky of smart city bluer? Evidence from satellite monitoring data. *J. Environ. Manag.* 317 (September), 115483 <https://doi.org/10.1016/j.jenvman.2022.115483>.
- Gharehchopogh, Farhad Soleimanian, Gholizadeh, Hojjat, 2019. A comprehensive survey: whale optimization algorithm and its applications. *Swarm Evolut. Comput.* 48 (August), 1–24. <https://doi.org/10.1016/j.swevo.2019.03.004>.
- Gulcebi, Medine I., Bartolini, Emanuele, Lee, Omay, Ligasras, Christos Panagiotis, Onat, Filiz, Mifsud, Janet, Striano, Pasquale, et al., 2021. Climate change and epilepsy: insights from clinical and basic science studies. *Epilepsy Behav.* 116 (March), 107791 <https://doi.org/10.1016/j.yebeh.2021.107791>.
- Guler, Dogus, Yomralioğlu, Tahsin, 2021. A reformative framework for processes from building permit issuing to property ownership in Turkey. *Land Use Policy* 101 (February), 105115. <https://doi.org/10.1016/j.landusepol.2020.105115>.
- Huang, Qiuping, Huang, Jiejun, Yang, Xining, Fang, Chuanglin, Liang, Youjin, 2019. Quantifying the seasonal contribution of coupling urban land use types on urban heat island using land contribution index: a case study in Wuhan, China. *Sustain. Cities Soc.* 44 (January), 666–675. <https://doi.org/10.1016/j.scs.2018.10.016>.
- Huo, Tengfei, Li, Xiaohui, Cai, Weiguang, Zuo, Jian, Jia, Fuyuan, Wei, Haifeng, 2020. Exploring the impact of urbanization on urban building carbon emissions in China: evidence from a provincial panel data model. *Sustain. Cities Soc.* 56 (May), 102068 <https://doi.org/10.1016/j.scs.2020.102068>.
- Jiang, Huiping, Sun, Zhongchang, Guo, Huadong, Weng, Qihao, Wenjie, Du, Xing, Qiang, Cai, Guoyin, 2021. An assessment of urbanization sustainability in China between 1990 and 2015 using land use efficiency indicators. *Npj Urb. Sustain.* 1 (1), 34. <https://doi.org/10.1038/s42949-021-00032-y>.
- Joshua, Udi, Bekun, Festus Victor, Sarkodie, Samuel Asumadu, 2020. New insight into the causal linkage between economic expansion, FDI, coal consumption, pollutant emissions and urbanization in South Africa. *Environ. Sci. Pollut. Res.* 27 (15), 18013–18024. <https://doi.org/10.1007/s11356-020-08145-o>.
- Kafy, Abdulla-Al, Abdullah-Al-Faisal, Shahinoor Rahman, Md., Islam, Muhamaimul, Al Rakib, Arshadul Islam, Md., Khan, Md. Hasib Hasan, et al., 2021. Prediction of seasonal urban thermal field variance index using machine learning algorithms in Cumilla, Bangladesh. *Sustain. Cities Soc.* 64 (January), 102542 <https://doi.org/10.1016/j.scs.2020.102542>.
- Kafy, Abdulla-Al, Saha, Milan, Faisal, Abdullah-Al-, Rahaman, Zulayyadini A., Rahman, Muhammad Tauhidur, Desheng Liu, Md., Fattah, Abdul, et al., 2022. Predicting the impacts of land use/land cover changes on seasonal urban thermal characteristics using machine learning algorithms. *Build. Environ.* 217 (June), 109066 <https://doi.org/10.1016/j.buildenv.2022.109066>.
- Kaveh, A., Ilchi Ghazaan, M., 2017. Enhanced whale optimization algorithm for sizing optimization of skeletal structures. *Mech. Based Des. Struct. Mach.* 45 (3), 345–362. <https://doi.org/10.1080/15397734.2016.1213639>.
- Le, Ho, Lee, and Jung., 2019. Application of long short-term memory (LSTM) neural network for flood forecasting. *Water* 11 (7), 1387. <https://doi.org/10.3390/w11071387>.
- Levine, Marl D., Steele, Robert V., 2021. Climate change: what we know and what is to be done. *WIREs Energy Environ.* 10 (1) <https://doi.org/10.1002/wene.388>.
- Li, Jiangang, Lei, Jun, Li, Songhong, Yang, Zhen, Tong, Yanjun, Zhang, Shubao, Duan, Zuliang, 2022. Spatiotemporal analysis of the relationship between urbanization and the eco-environment in the Kashgar metropolitan area, China. *Ecol. Indic.* 135 (February), 108524 <https://doi.org/10.1016/j.ecolind.2021.108524>.
- Liu, Xin, Wang, Ping, Song, Hang, Zeng, Xiaoying, 2021. Determinants of net primary productivity: low-carbon development from the perspective of carbon sequestration. *Technol. Forecast. Soc. Chang.* 172 (November), 121006 <https://doi.org/10.1016/j.techfore.2021.121006>.
- Luo, Xilian, Chuck Wah, Yu, Zhou, Dian, Zhaolin, Gu., 2019. Challenges and adaptation to urban climate change in China: a viewpoint of urban climate and urban planning. *Indoor Built Environ.* 28 (9), 1157–1161. <https://doi.org/10.1177/1420326X19867187>.
- Mirjalili, Seyedali, Lewis, Andrew, 2016. The whale optimization algorithm. *Adv. Eng. Softw.* 95 (May), 51–67. <https://doi.org/10.1016/j.advengsoft.2016.01.008>.
- Miyamoto, Motoe, 2020. Poverty reduction saves forests sustainably: lessons for deforestation policies. *World Dev.* 127 (March), 104746 <https://doi.org/10.1016/j.worlddev.2019.104746>.
- Mohammad, Pir, Goswami, Ajanta, Chauhan, Sarthak, Nayak, Shailesh, 2022. Machine learning algorithm based prediction of land use land cover and land surface temperature changes to characterize the surface urban heat island phenomena over Ahmedabad City, India. *Urban Clim.* 42 (March), 101116 <https://doi.org/10.1016/j.ulclim.2022.101116>.
- Pour, Mozaffaree, Najmeh, and Tönu Oja., 2021. Urban expansion simulated by integrated cellular automata and agent-based models; an example of Tallinn, Estonia. *Urban Sci.* 5 (4), 85. <https://doi.org/10.3390/urbansci5040085>.
- Rahman, M. Tauhid Ur, Esha, Eshrat Jahan, 2020. Prediction of Land Cover Change Based on CA-ANN Model to Assess Its Local Impacts on Bagerhat, Southwestern Coastal Bangladesh. *Geocarto International*, pp. 1–23. <https://doi.org/10.1080/10106049.2020.1831621>. October.
- Rana, Nadim, Latiff, Muhammad Shafiq Abd, Shafi'i Muhammad Abdulhamid, and Haruna Chiroma., 2020. Whale optimization algorithm: a systematic review of contemporary applications, modifications and developments. *Neural Comput. & Appl.* 32 (20), 16245–16277. <https://doi.org/10.1007/s00521-020-04849-z>.
- Rao, Yingxue, Zhou, Jiang, Zhou, Min, He, Qingsong, Jiayu, Wu., 2020. Comparisons of three-dimensional urban forms in different urban expansion types: 58 sample cities in China. *Growth Chang.* 51 (4), 1766–1783. <https://doi.org/10.1111/grow.12426>.
- Rao, Yingxue, Dai, Jingyi, Dai, Deyi, He, QingSong, 2021. Effect of urban growth pattern on land surface temperature in China: a multi-scale landscape analysis of 338 cities. *Land Use Policy* 103 (April), 105314. <https://doi.org/10.1016/j.landusepol.2021.105314>.
- Ren, Zhibin, Yao, Fu, Yunxia, Du, Zhao, Hongbo, 2019. Spatiotemporal patterns of urban thermal environment and comfort across 180 cities in summer under China's rapid urbanization. *PeerJ* 7 (August), e7424. <https://doi.org/10.7717/peerj.7424>.
- Sarkar, Debabrata, Sarkar, Trishna, Saha, Sunil, Mondal, Prolay, 2021. Compiling non-parametric tests along with CA-ANN model for precipitation trends and variability analysis: a case study of eastern India. *Water Cycle* 2, 71–84. <https://doi.org/10.1016/j.watcyc.2021.11.002>.
- Shaker, Richard R., Altman, Yaron, Deng, Chengbin, Vaz, Eric, Wayne Forsythe, K., 2019. Investigating urban Heat Island through spatial analysis of New York City streetscapes. *J. Clean. Prod.* 233 (October), 972–992. <https://doi.org/10.1016/j.jclepro.2019.05.389>.
- Shen, Maocai, Huang, Wei, Chen, Ming, Song, Biao, Zeng, Guangming, Zhang, Yaxin, 2020. (Micro)plastic crisis: un-ignorable contribution to global greenhouse gas emissions and climate change. *J. Clean. Prod.* 254 (May), 120138 <https://doi.org/10.1016/j.jclepro.2020.120138>.
- Sherstinsky, Alex, 2020. Fundamentals of recurrent neural network (RNN) and long short-term memory (LSTM) network. *Phys. D Nonlin. Phenom.* 404 (March), 132306 <https://doi.org/10.1016/j.physd.2019.132306>.
- Song, Junnian, Yang, Wei, Wang, Shuo, Xian'en Wang, Yoshiro Higano, and Kai Fang., 2018. Exploring potential pathways towards fossil energy-related GHG emission peak prior to 2030 for China: an integrated input-output simulation model. *J. Clean. Prod.* 178 (March), 688–702. <https://doi.org/10.1016/j.jclepro.2018.01.062>.
- Stewart, Iain D., 2019. Why should urban Heat Island researchers study history? *Urban Clim.* 30 (December), 100484 <https://doi.org/10.1016/j.ulclim.2019.100484>.
- Tan, Shukui, Zhang, Maomao, Wang, Ao, Zhang, Xuesong, Chen, Tianchi, 2021. How do varying socio-economic driving forces affect China's carbon emissions? New evidence from a multiscale geographically weighted regression model. *Environ. Sci. Pollut. Res.* 28 (30), 41242–41254. <https://doi.org/10.1007/s11356-021-13444-1>.
- Tariq, Aqil, Shu, Hong, 2020. CA-Markov chain analysis of seasonal land surface temperature and land use land cover change using optical multi-temporal satellite data of Faisalabad, Pakistan. *Remote Sens.* 12 (20) <https://doi.org/10.3390/rs12203402>.

- Tian, Xin, Bai, Fuli, Jia, Jinhua, Liu, Yang, Shi, Feng, 2019. Realizing low-carbon development in a developing and industrializing region: impacts of industrial structure change on CO₂ emissions in Southwest China. *J. Environ. Manag.* 233 (March), 728–738. <https://doi.org/10.1016/j.jenvman.2018.11.078>.
- Verbić, Miroslav, Satrović, Elma, Muslija, Adnan, 2021. Environmental Kuznets curve in southeastern Europe: the role of urbanization and energy consumption. *Environ. Sci. Pollut. Res.* 28 (41), 57807–57817. <https://doi.org/10.1007/s11356-021-14732-6>.
- Wan, Jikang, Zhu, Min, Ding, Wei, 2021. "Accuracy evaluation and parameter analysis of land surface temperature inversion algorithm for Landsat-8 data." Edited by Stefania Bonafoni. *Adv. Meteorol.* 2021 (September), 1–16. <https://doi.org/10.1155/2021/9917145>.
- Wang, Bin, Luo, Lei, 2022. Service value of a Bay City ecosystem based on green buildings and landscape pattern changes. *Sustainable Computing: Informatics and Systems* 35 (September), 100758. <https://doi.org/10.1016/j.suscom.2022.100758>.
- Wang, Shaojian, Zeng, Jingyuan, Huang, Yongyuan, Shi, Chenyi, Zhan, Peiyu, 2018. The effects of urbanization on CO₂ emissions in the Pearl River Delta: a comprehensive assessment and panel data analysis. *Appl. Energy* 228 (October), 1693–1706. <https://doi.org/10.1016/j.apenergy.2018.06.155>.
- Wang, Shaojian, Shi, Chenyi, Fang, Chuanglin, Feng, Kuishuang, 2019. Examining the spatial variations of determinants of energy-related CO₂ emissions in China at the City level using geographically weighted regression model. *Appl. Energy* 235 (February), 95–105. <https://doi.org/10.1016/j.apenergy.2018.10.083>.
- Wang, Ying, Zhang, Qi, Bilsborrow, Richard, Tao, Shiqi, Chen, Xiaodong, Sullivan-Wiley, Kira, Huang, Qingfeng, Li, Jiangfeng, Song, Conghe, 2020. Effects of payments for ecosystem services programs in China on rural household labor allocation and land use: identifying complex pathways. *Land Use Policy* 99 (December), 105024. <https://doi.org/10.1016/j.landusepol.2020.105024>.
- Xiong, Guojiang, Zhang, Jing, Shi, Dongyuan, He, Yu, 2018. Parameter extraction of solar photovoltaic models using an improved whale optimization algorithm. *Energy Convers. Manag.* 174 (October), 388–405. <https://doi.org/10.1016/j.enconman.2018.08.053>.
- Xu, Ningke, Wang, Xiangqian, Meng, Xiangrui, Chang, Haoqian, 2022. Gas concentration prediction based on IWOA-LSTM-CEEMDAN residual correction model. *Sensors* 22 (12), 4412. <https://doi.org/10.3390/s22124412>.
- Yang, Kun, Zhenyu, Yu, Luo, Yi, Yang, Yang, Zhao, Lei, Zhou, Xiaolu, 2018. Spatial and temporal variations in the relationship between lake water surface temperatures and water quality - a case study of Dianchi Lake. *Sci. Total Environ.* 624, 859–871. <https://doi.org/10.1016/j.scitotenv.2017.12.119>.
- Yang, Kun, Zhenyu, Yu, Luo, Yi, Zhou, Xiaolu, Shang, Chunxue, 2019. Spatial-temporal variation of lake surface water temperature and its driving factors in Yunnan-Guizhou plateau. *Water Resour. Res.* 55, 4688–4703. <https://doi.org/10.1029/2019WR025316>.
- Yang, Shaomei, Chen, Dongjiu, Li, Shengli, Wang, Weijun, 2020a. Carbon price forecasting based on modified ensemble empirical mode decomposition and long short-term memory optimized by improved whale optimization algorithm. *Sci. Total Environ.* 716 (May), 137117 <https://doi.org/10.1016/j.scitotenv.2020.137117>.
- Yang, Kun, Zhenyu, Yu, Luo, Yi, 2020b. Analysis on driving factors of lake surface water temperature for major lakes in Yunnan-Guizhou plateau. *Water Res.* 184, 116018 <https://doi.org/10.1016/j.watres.2020.116018>.
- Yatoo, Saleem Ahmad, Sahu, Paulami, Kalubarme, Manik H., Kansara, Bhagirath B., 2022. Monitoring land use changes and its future prospects using cellular automata simulation and artificial neural network for Ahmedabad City, India. *GeoJournal* 87 (2), 765–786. <https://doi.org/10.1007/s10708-020-10274-5>.
- Zhang, M., Tan, S., Zhang, X., 2022. How do varying socio-economic factors affect the scale of land transfer? evidence from 287 cities in China. *Environ. Sci. Pollut. Res.* 29, 40865–40877. <https://doi.org/10.1007/s11356-021-18126-6>.
- Zhang, Hao, Tang, Lei, Yang, Chen, Lan, Shulin, 2019. Locating electric vehicle charging stations with service capacity using the improved whale optimization algorithm. *Adv. Eng. Inform.* 41 (August), 100901 <https://doi.org/10.1016/j.aei.2019.02.006>.
- Zhang, M., Kafy, A.-A., Ren, B., Zhang, Y., Tan, S., Li, J., 2022. Application of the optimal parameter geographic detector model in the identification of influencing factors of ecological quality in Guangzhou, China. *Land* 11. <https://doi.org/10.3390/land11081303>.
- Zhang, Maomao, Tan, Shukui, Pan, Zichun, Hao, Daoqing, Zhang, Xuesong, Chen, Zhenhuan, 2022a. The spatial spillover effect and nonlinear relationship analysis between land resource misallocation and environmental pollution: evidence from China. *J. Environ. Manag.* 321 (November), 115873 <https://doi.org/10.1016/j.jenvman.2022.115873>.
- Zhang, Maomao, Tan, Shukui, Yanwei Zhang, Ju, He, and Qianlin Ni., 2022b. Does land transfer promote the development of new-type urbanization? New evidence from urban agglomerations in the middle reaches of the Yangtze River. *Ecol. Indic.* 136 (March), 108705 <https://doi.org/10.1016/j.ecolind.2022.108705>.
- Zhang, X., Zhang, M., He, J., Wang, Q., Li, D., 2019. The spatial-temporal characteristics of cultivated land and its influential factors in the low hilly region: a case study of Lishan Town, Hubei Province, China. *Sustain* 11, 1–18. <https://doi.org/10.3390/su11143810>.
- Zhang, Maomao, Zhang, Cheng, Kafy, Abdulla-Al, Tan, Shukui, 2022c. Simulating the relationship between land use/cover change and urban thermal environment using machine learning algorithms in Wuhan City, China. *Land* 11 (1). <https://doi.org/10.3390/land11010014>.
- Zhao, Chunhong, Weng, Qihao, Hersperger, Anna M., 2020. Characterizing the 3-D urban morphology transformation to understand urban-form dynamics: a case study of Austin, Texas, USA. *Landsc. Urban Plan.* 203 (November), 103881 <https://doi.org/10.1016/j.landurbplan.2020.103881>.